Journal of Magnetic Resonance **155,** 123–130 (2002)
doi:10.1006/jmre.2002.2514, available online at http://www.idealibrary.com on IDEAL®

COMMUNICATIONS

Evaluation and Optimization of Coherence Transfer in High Molecular Weight Systems

Perttu Permi*,[1] and Arto Annila†

*NMR Laboratory, Institute of Biotechnology, P.O. Box 56, FIN-00014, University of Helsinki, Helsinki, Finland; and †Department of Physics, P.O. Box 64, FIN-00014, University of Helsinki, Helsinki, Finland

Received September 28, 2001; revised December 27, 2001

For very large proteins in the highest magnetic fields, the large chemical shift anisotropy (CSA) of carbonyl carbon deteriorates coherence transfer efficiency in experiments designed for unambiguous sequential backbone assignment. In this communication, coherence throughput of several TROSY experiments is evaluated. Two new experiments, MP-HNCA and HN(CO)CANH, are also introduced as attractive alternatives for sequential assignment purposes of large proteins with correlation time over 50 ns. Their theoretical coherence transfer efficiencies for the interresidual $^{13}C^{\alpha}$ correlations are significantly better than in recently introduced MP-CT-HNCA and sequential HNCA experiments. The improvement with the new experiments is observed already on 60.8 kDa homodimer of protein Cel6A at 800 ^{1}H MHz. © 2002 Elsevier Science (USA)

Key Words: **assignment; coherence transfer; HNCA; spin-state selection; TROSY.**

Assignment of chemical shifts to individual atoms is of course imperative for any detailed structural study by high-resolution NMR spectroscopy. In protein NMR spectroscopy, rapid development during the past decade in both sample production and methodological innovations, as well as improvement in instruments, has extended the size-limit of proteins amenable to sequential assignment from 10 kDa to 100 kDa size-regime (*1*). The production of ^{15}N, ^{13}C enriched protein samples enabled the use of so-called triple-resonance spectroscopy for the chemical shift assignment of ^{1}H, ^{15}N, and ^{13}C spins from 15–25 kDa weight proteins (*2–3*). It was realized, however, that the assignment of larger proteins (>25 kDa) requires perdeuteration, i.e., substitution of aliphatic protons with deuterons in order to slow $^{13}C^{\alpha}$ as well as $^{1}H^{N}$ relaxation (*4*). The transverse relaxation optimized spectroscopy (TROSY) (*5*) and its subsequent modifications and improvements have pushed the size limit over 100 kDa (*6*).

A number of slightly different methods for the chemical shift assignment of protein main chain resonances have been introduced over the past several years (*2, 3, 7–12*). Customarily complete assignment of chemical shifts employing a set of H^{N} detected three-dimensional experiments, i.e., (CT)-HNCA and (CT)-HNCACB, are used to connecting both intraresidual and sequential $^{13}C^{\alpha}$ and $^{13}C^{\beta}$ resonances with intraresidual ^{15}N and $^{1}H^{N}$ resonances (*3*). However, due to the comparable sizes of $^{1}J_{NC^{\alpha}}$ and $^{2}J_{NC^{\alpha}}$ couplings it is not always clear which of the $^{1}H^{N}(i)$, $^{15}N(i)$, $^{13}C^{\alpha}$ cross peaks belong to $^{13}C^{\alpha}(i)$ and $^{13}C^{\alpha}(i-1)$. In most of the cases, the $^{1}J_{NC^{\alpha}}$, i.e., the intraresidual cross peak is more intense compared to interresidual cross peak, but unfortunately contradictionary results are also probable. To ensure unambiguous assignment of intra- and interresidual ^{15}N, $^{13}C^{\alpha}$ connectivities, the HN(CO)CA and HN(CO)CACB experiments are usually recorded, showing only sequential ^{15}N, $^{13}C^{\alpha}$ cross peaks. In addition to interresidual selectivity of the HN(CO)CA type of experiments, they usually exhibit higher sensitivity than their corresponding counterparts based on the HNCA building blocks due to larger $^{1}J_{NC'}$ and $^{1}J_{C'C^{\alpha}}$ couplings used for magnetization transfer from $^{1}H^{N}$ to $^{13}C^{\alpha}$ and back. Especially the $^{13}C'$ spin is excellent for the relay of magnetization in smaller proteins owing to its favorable relaxation properties and its large (~53 Hz) coupling to the preceding $^{13}C^{\alpha}$ spin.

However, this strategy began to fail for large proteins at high magnetic fields (*6, 12, 13*). Carbonyl carbon has very large chemical shift anisotropy and consequently the transverse relaxation rate of the carbonyl carbon increases very rapidly as the polarizing magnetic field strength as well as protein size get larger (*13*). The rate of the $^{13}C'$ transverse relaxation has quadratic dependence on the magnetic field strength, and consequently the NMR experiments utilizing $^{13}C'$ spin are best carried out at field strength smaller than 600 MHz proton frequency (*12, 13*). It has been shown that for the protein size of 110 kDa the rapid $^{13}C'$ relaxation deteriorates the HN(CO)CA experiment with respect to HNCA already at 500 MHz (*6*). This is particularly unfortunate as the TROSY spectroscopy works best at the highest magnetic fields available today while the $^{13}C'$ relaxation ruins the HN(CO)CA and HN(CO)CACB experiments.

[1] To whom correspondence should be addressed. Fax: +358-9-191-595-41. E-mail: Perttu.Permi@helsinki.fi.

1090-7807/02 $35.00

To address this problem, we recently introduced a new approach, the MP-CT-HNCA experiment, for sequential assignment, enabling main chain assignment without HN(CO)CA or HN(CO)CACB experiments (*12*). The key issue, i.e., to distinguish between the intra- and interresidual connectivities without using the HN(CO)CA experiment, was accomplished by employing spin-state-selective filtering (*14–17*) in the $^{13}C^{\alpha}$-dimension with respect to interresidual $^{13}C'(i-1)$ spin. The intraresidual cross peaks could then be separated from interresidual cross peaks by the size of $^{1}J_{C^{\alpha}(i-1)C'(i-1)}$ and $^{2}J_{C^{\alpha}(i)C'(i-1)}$ couplings. The $^{1}J_{C^{\alpha}(i-1)C'(i-1)}$ coupling is at least an order of magnitude larger than $^{2}J_{C^{\alpha}(i)C'(i-1)}$ and consequently interresidual cross peaks can be easily recognized even when the resolution is not sufficient for resolving ~50–55 Hz coupling. An alternative method for sequential assignment, sequential HNCA, was presented by Meissner and Sørensen (*18*). The method utilizes large $^{1}J_{C^{\alpha}C'}$ coupling during a constant time (CT) period, t_1, in order to refocus antiphase $^{1}J_{C^{\alpha}C'}$ coupling for sequential connectivities, whereas the intraresidual $^{13}C^{\alpha}$'s remain intact or defocus to double antiphase form. Thus, in practice only the sequential cross peaks are converted into observable magnetization.

Unfortunately, both the MP-CT-HNCA and sequential HNCA experiments have one major drawback hampering their performance with respect to the conventional HN(CO)CA experiment. Both experiments suffer from the constant time period during which the $^{13}C^{\alpha}$ chemical shift is labeled and $^{1}J_{C^{\alpha}C'}$ coupling is modulated (MP-CT-HNCA) or refocused (sequential HNCA). In fact, sensitivity losses during this period can be larger than gains from redirecting the coherence transfer to $^{13}C^{\alpha}$ spin, i.e., from avoiding coherence transfer via carbonyl carbon.

The purpose of this paper is first to evaluate relative coherence transfer efficiencies for the sequential connectivities and compare attainable sensitivity for the MP-CT-HNCA, sequential HNCA, CT-HN(CO)CA, and HN(CO)CA experiments in the case of very large protein at 800 ^{1}H MHz. Second, we introduce two alternative methods, namely a variant of the MP-HNCA experiment and a novel HN(CO)CANH experiment, which is a hybrid of the familiar HNCA and HN(CO)CA experiments. Both experiments provide significantly improved sensitivity over the MP-CT-HNCA, sequential HNCA, and CT-HN(CO)CA experiments and prove to be attractive choices for the HN(CO)CA experiment in high-molecular-weight systems.

Let us first focus on differences between the original MP-CT-HNCA, sequential HNCA, CT-HN(CO)CA, and HN(CO)CA experiments shown in Figs. 1a–1d. This can be most conveniently accomplished by inspecting coherence transfer pathways for the differing parts for each experiment. It is worth mentioning that presented pulse schemes differ somewhat from the original versions, for instance, by the implementation of the TROSY selection introduced by Yang and Kay (*19*). To make possible straightforward evaluation of coherence transfer throughputs, we implemented the experiments with identical coherence transfer pathway selection.

The coherence transfer efficiencies for the *interresidual* cross peaks in the original MP-CT-HNCA experiment,

$$\sin^2\left(2\pi^2 J_{NC^{\alpha}} T_a\right)\cos^2\left(2\pi^1 J_{NC^{\alpha}} T_a\right)\sin\left(2\pi^1 J_{NC'} T_b\right) \times \cos\left(2\pi^1 J_{C^{\alpha}C^{\beta}} T_c\right)\exp\left(-2(T_a+T_b)/T_{2N}\right)\exp\left(-2T_c/T_{2C^{\alpha}}\right), \quad [1]$$

and in the sequential HNCA experiment,

$$\sin^2\left(2\pi^2 J_{NC^{\alpha}} T_a\right)\cos^2\left(2\pi^1 J_{NC^{\alpha}} T_a\right)\sin\left(2\pi^1 J_{C^{\alpha}C'} T_c\right) \times \cos\left(2\pi^1 J_{C^{\alpha}C^{\beta}} T_c\right)\exp\left(-4T_a/T_{2N}\right)\exp\left(-2T_c/T_{2C^{\alpha}}\right), \quad [2]$$

are rather similar. The nominal values for the coupling constants and delays in Eqs. [1], [2] are $^{1}J_{NC^{\alpha}} = 10$ Hz, $^{2}J_{NC^{\alpha}} = 7$ Hz, $^{1}J_{NC'} = 15$ Hz, $^{1}J_{C'C^{\alpha}} = 53$ Hz, $^{1}J_{C^{\alpha}C^{\beta}} = 35$ Hz, $2T_a \sim 25$ ms, $2T_b \sim 33$ ms, $2T_c \sim 7$ ms. In the MP-CT-HNCA experiment, the delay $2T_b$ is matched to $1/(2J_{NC'})$, because it is employed for the spin-state selection. In addition, the coupling between $^{13}C^{\alpha}$ and $^{13}C'$ spins is not refocused during t_1 (*12*). In the case of sequential HNCA, the coupling between $^{13}C^{\alpha}$ and $^{13}C'$ spins evolves during the $2T_c$ period. Therefore, the ^{15}N transverse relaxation is effective for a longer period in the MP-CT-HNCA experiment, whereas the $2T_c$ period is a compromise between $^{1}J_{C^{\alpha}C'}$ and $^{1}J_{C^{\alpha}C^{\beta}}$ couplings in the sequential HNCA experiment (*18*).

When we assume that the transverse relaxation rates for the ^{15}N, $^{13}C'$ and $^{13}C^{\alpha}$ spins, in a very large system at the highest magnetic field currently available (900 ^{1}H MHz), are 50, 6, and 20 ms, respectively, the corresponding coherence transfer efficiencies for *the first* t_1 *increment* ($t_1 = 0$) in the *in-phase* MP-CT-HNCA and sequential HNCA experiments are 0.022 and 0.020. When $^{1}J_{NC^{\alpha}}$ and $^{2}J_{NC^{\alpha}}$ are comparable in size, 10 Hz and 9 Hz, respectively, the corresponding coherence transfer efficiencies for those residues are 0.034 and 0.031 (Fig. 2a). For the sake of clarity, we wish to emphasize that in the MP-CT-HNCA experiment two spectra, which are either *in-phase* or *antiphase* with respect to the interresidual $^{13}C'$ in t_1, are recorded. When the $t_{1,\max}$ is short, ~7 ms, the *in-phase* experiment resembles the conventional CT-HNCA experiment. Thus, it can be used for sequential assignment in the usual way, which is also preferable because the inherent sensitivity of the *in-phase* experiment is $\sim\sqrt{2}$ higher than the subspectra (*12*). If the intensities of intra- and interresidual cross peaks are similar, then the addition or subtraction of these two experiments reveals whether the cross peak originates from intra- or interresidual connectivity, because $^{1}J_{C^{\alpha}(i-1)C'(i-1)} \gg {}^{2}J_{C^{\alpha}(i)C'(i-1)}$. Likewise, if the $t_{1,\max}$ is longer than ~7–9 ms, the sensitivity of the *in-phase* MP-CTHNCA experiment is reduced by $\sim\sqrt{2}$ due to resolved $^{1}J_{C^{\alpha}C'}$ coupling.

Now, let us elaborate on coherence transfer efficiencies in the CT-HN(CO)CA and conventional, i.e., (non-CT)

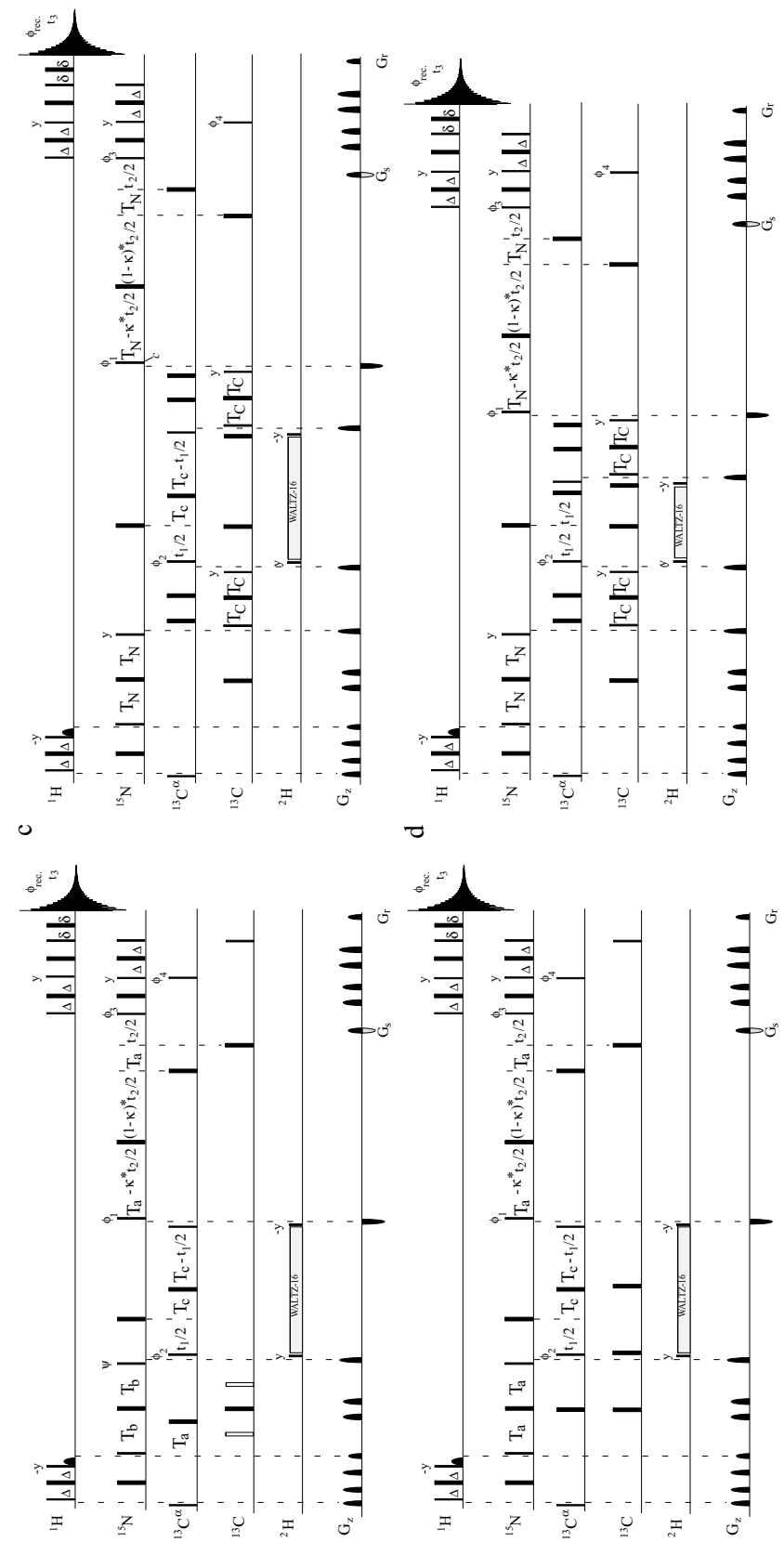

FIG. 1. The MP-CTHNCA (a), sequential HNCA (b), CT-HN(CO)CA (c), and HN(CO)CA (d) experiments for sequential assignment. Narrow and wide bars correspond to 90° and 180° flip angles, respectively, applied with phase x unless otherwise indicated. Half-ellipses denote water-selective 90° pulses to obtain water-flip-back (*23*, *24*). All 90° (180°) pulses for $^{13}C'$ and $^{13}C^{\alpha}$ are applied with a strength of $\Omega/\sqrt{15}$ ($\Omega/\sqrt{3}$), where Ω is the frequency difference between the centers of the $^{13}C'$ and $^{13}C^{\alpha}$ regions. The ^{1}H, ^{15}N, $^{13}C'$ and $^{13}C^{\alpha}$ carrier positions are 4.7 (water), 120 (center of ^{15}N spectral region), 175 ppm (center of $^{13}C'$ spectral region), and 55 ppm (center of $^{13}C^{\alpha}$ spectral region), respectively. Deuterium is decoupled using the WALTZ-16 sequence (*25*). All $^{13}C^{\alpha}$ pulses were applied on-resonance and $^{13}C'$ pulses off-resonance with phase modulation by Ω in pulse sequences (a) and (b). In the schemes (c) and (d), the ^{13}C transmitter is set to initially to the $^{13}C'$ region and is later shifted to 55 ppm just before the 90° ϕ_2 pulse and shifted back to 176 ppm after the 90°($^{13}C^{\alpha}$) pulse ensuing the t_1 period. Frequency discrimination in F_2 is obtained using the sensitivity-enhanced TROSY with gradient selection (*19*) by inverting the sign of the G_s gradient pulse together with the inversion of ϕ_3. Quadrature detection in the $^{13}C^{\alpha}$ dimension is obtained by States-TPPI (*26*) applied to ϕ_2. Pulsed field gradients were inserted as indicated for coherence transfer pathway selection and residual water suppression. The nominal delay durations are $\Delta = 1/(4J_{HN})$; $T_b = T_N = 1/(4J_{NC'})$; $T_a = 1/(8J_{NC^{\alpha}}) = \sim 25$ ms; $T_C = 1/(4J_{C'C^{\alpha}})$; δ = gradient + field recovery delay; $T_c = 1/(8J_{C^{\alpha}C^{\beta}})$; $0 \le \kappa \le T_a/t_{2,max}$ (schemes a and b); $0 \le \kappa \le T_N/t_{2,max}$ (schemes c and d). Gradient strengths (durations): $G_s = 30$ G/cm (1.25 ms), $G_r = 29.6$ G/cm (0.125 ms). (a) Phase cycling for the in-phase MP-CT-HNCA spectrum is $\phi_1 = y$; $\phi_2 = x, -x$; $\phi_3 = x$; $\phi_4 = 2(x), 2(-x)$; $\phi_{rec.} = x, -x$; $\psi = y$. For the antiphase spectrum, ψ is incremented by 90°. The last 90°($^{13}C^{\alpha}$) pulse removes the dispersive contribution from the lineshape (*17*, *27*, *28*). The last 90° pulse on $^{13}C'$ removes the E.COSY pattern (*17*). (b) Phase cycling for the sequential HNCA experiment: $\phi_1 = y$; $\phi_2 = y, -y$; $\phi_3 = x$; $\phi_4 = 2(x), 2(-x)$; $\phi_{rec.} = x, -x$. (c, d) Phase cycling for the CT-HN(CO)CA and HN(CO)CA schemes: $\phi_1 = y$; $\phi_2 = x, -x$; $\phi_3 = x$; $\phi_4 = 2(x), 2(-x)$; $\phi_{rec.} = x, -x$.

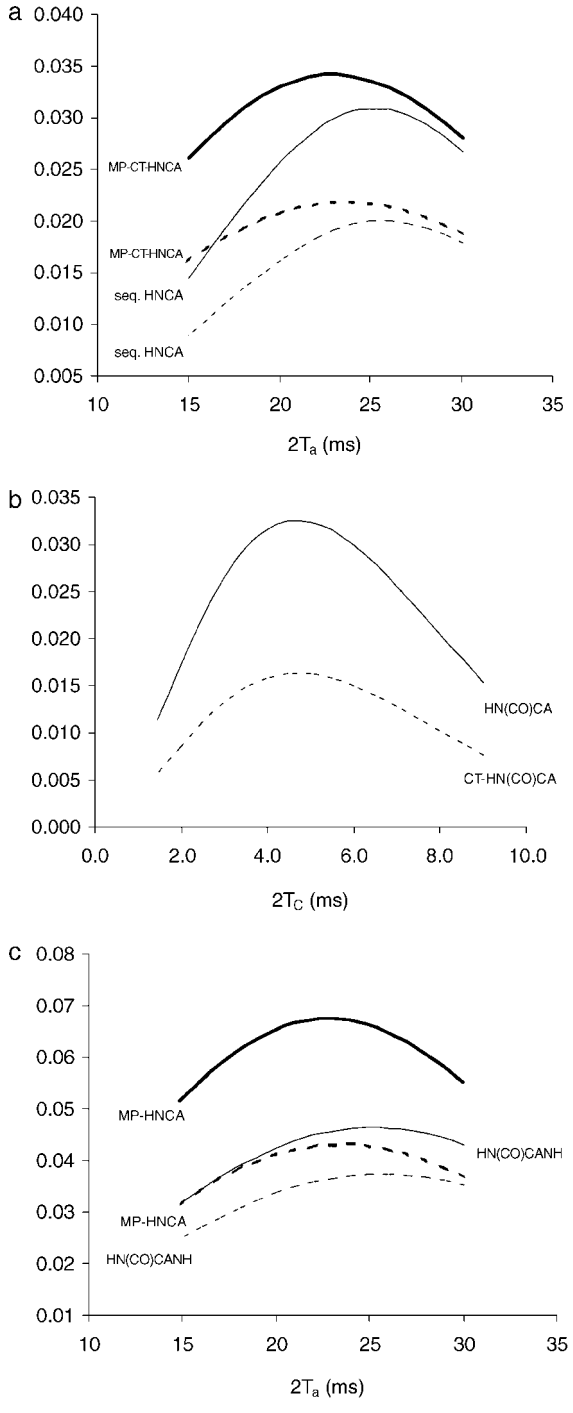

FIG. 2. Coherence transfer efficiencies, for the first increment, as a function of $2T_a$ for the MP-CT-HNCA (a) and sequential HNCA (a) experiments, and as a function of $2T_C$ for the CT-HN(CO)CA (b) and HN(CO)CA (b) experiments. The transfer functions were calculated according to Eqs. [1]–[6], respectively, using the following parameters: $T_{2N} = 50$ ms, $T_{2C'} = 6$ ms, $T_{2C^\alpha} = 20$ ms, $2T_N = 25$ ms, $2T_b = 33$ ms, $2T_c = 7$ ms, ${}^1J_{NC'} = 15$ Hz, ${}^1J_{NC^\alpha} = 10$ Hz, ${}^2J_{NC^\alpha} = 9$ Hz (7 Hz for dashed line), ${}^1J_{C'C^\alpha} = 53$ Hz, ${}^1J_{C^\alpha C^\beta} = 35$ Hz. The corresponding transfer efficiencies for the proposed MP-HNCA and HN(CO)CANH experiments with respect to $2T_a$ are shown in plot (c). Functions in Eqs. [5], [6] were plotted using the values described above except for $2T_C = 4.5$ ms in the case of HN(CO)CANH.

HN(CO)CA experiments. Both experiments use ${}^1J_{NC'}$ coupling for transferring magnetization from the ^{15}N spin to the preceding ^{13}C′ spin. This is followed by the INEPT-type transfer from ^{13}C′ to the $^{13}C^\alpha$ spin, which is rather inefficient in very large proteins as discussed more throughly in the original paper (*12*). Subsequent t_1 period is either implemented as a constant-time or real-time evolution. The former is rather costly in larger proteins whose $^{13}C^\alpha$ spin transverse relaxation is rapid despite of perdeuteration (*11*). The coherence transfer efficiency depends on

$$\sin^2(2\pi {}^1J_{NC'}T_N)\sin^2\left(2\pi {}^1J_{C'C^\alpha}T_C\right)\cos\left(2\pi {}^1J_{C^\alpha C^\beta}T_c\right) \times \exp\left(-2T_c/T_{2C^\alpha}\right)\exp(-4T_N/T_{2N})\exp(-4T_C/T_{2C'}) \quad [3]$$

in the CT-HN(CO)CA experiment and

$$\sin^2(2\pi {}^1J_{NC'}T_N)\sin^2\left(2\pi {}^1J_{C'C^\alpha}T_C\right)\cos\left(\pi {}^1J_{C^\alpha C^\beta}t_1\right) \times \exp(-4T_N/T_{2N})\exp(-4T_C/T_{2C'})\exp(-t_1/T_{2C^\alpha}) \quad [4]$$

in the HN(CO)CA experiment. The nominal values are: ${}^1J_{NC'} = 15$ Hz, ${}^1J_{C'C^\alpha} = 53$ Hz, $2T_N \sim 33$ ms, $2T_C \sim 9.1$ ms, $2T_c \sim 7$ ms. Again, using the same values for the ^{15}N, ^{13}C′, and $^{13}C^\alpha$ transverse relaxation rates as above, the coherence transfer efficiencies can be optimized, yielding values of 0.016 and 0.033 for the *first increment* in the CT-HN(CO)CA and HN(CO)CA experiments, respectively (Fig. 2b). Thus, it can be immediately realized that the sensitivity of the non-CT HN(CO)CA experiment is significantly better than that of its constant-time counterpart. It should be noted that ${}^1J_{C^\alpha C^\beta}$ modulation and $^{13}C^\alpha$ transverse relaxation during t_1 reduce the signal intensity in the HN(CO)CA experiment also. However, provided that $t_{1,\max}$ in the non-CT HN(CO)CA experiment is $<1/(3J_{C^\alpha C^\beta}) - 1/(2J_{C^\alpha C^\beta})$, i.e., ${}^1J_{C^\alpha C^\beta}$ coupling is not resolved, the sensitivity of the non-CT HN(CO)CA is ~2 higher than in the CT-HN(CO)CA experiment. If we now compare theoretical coherence transfer efficiencies between these four experiments, we can easily assure ourselves with the fact that coherence transfer is most efficient for the non-CT version of the HN(CO)CA experiment even in the case of very rapid ^{13}C′ transverse relaxation.

Fortunately, there are other possibilities to obtain sequential $^{13}C^\alpha$ correlations, namely variant of the original MP-CT-HNCA experiment, and the novel HN(CO)CANH experiment (Figs. 3a, 3b). Let us first concentrate on the MP-HNCA experiment (Fig. 3a). It is essentially the same experiment as the MP-CT-HNCA experiment except for the real-time $^{13}C^\alpha$ evolution in t_1. It is not the purpose of this paper to go through how the MP-CT-HNCA experiment works except for the relevant parts. Hence, we refer to the original paper for theoretical and experimental details concerning the MP-CT-HNCA experiment (*12*).

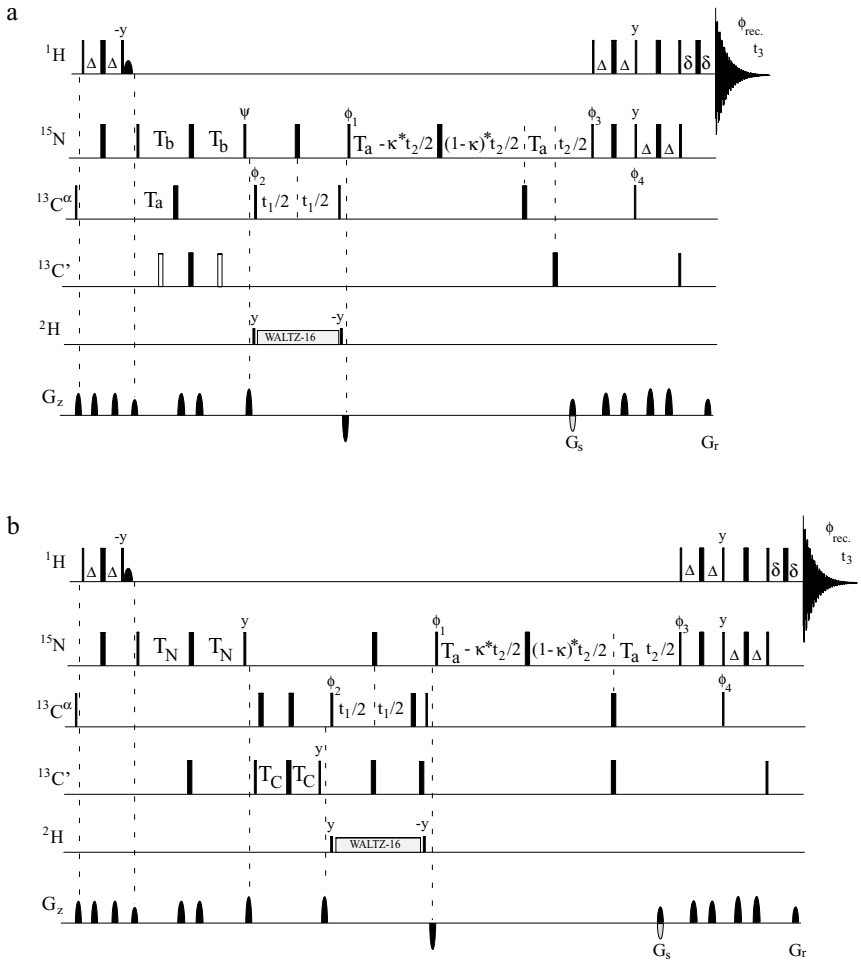

FIG. 3. The MP-HNCA (a) and HN(CO)CANH experiments for the sequential assignment. Narrow and wide bars correspond to 90° and 180° flip angles, respectively, applied with phase x unless otherwise indicated. All 90° (180°) pulses for $^{13}C'$ and $^{13}C^{\alpha}$ are applied with a strength of $\Omega/\sqrt{15}\,(\Omega/\sqrt{3})$, where Ω is the frequency difference between the centers of the $^{13}C'$ and $^{13}C^{\alpha}$ regions. Half-ellipses denote water-selective 90° pulses to obtain water flip-back (*24, 25*). The ^{1}H, ^{15}N, $^{13}C'$, and $^{13}C^{\alpha}$ carrier positions are 4.7 (water), 120 (center of ^{15}N spectral region), 175 ppm (center of $^{13}C'$ spectral region), and 55 ppm (center of $^{13}C^{\alpha}$ spectral region), respectively. All $^{13}C^{\alpha}$ pulses were applied on-resonance and $^{13}C'$ pulses off-resonance with phase modulation by Ω in the scheme (a). In the scheme (b), the ^{13}C transmitter is set to initially to the $^{13}C'$ region and is later shifted to 55 ppm just before the 90° ϕ_4 pulse. Frequency discrimination in F_2 is obtained using the sensitivity-enhanced TROSY with gradient selection (*19*) by inverting the sign of the G_s gradient pulse together with the inversion of ϕ_3. Quadrature detection in the $^{13}C^{\alpha}$ dimension is accomplished by States-TPPI (*26*) applied to ϕ_2. Pulsed field gradients were inserted as indicated for coherence transfer pathway selection and residual water suppression. The nominal delay durations are $\Delta = 1/(4J_{HN})$; $T_b = T_N = 1/(4J_{NC'})$; $T_a = 1/(8J_{NC^{\alpha}}) = \sim 25$ ms; $T_C = 1/(4J_{C'C^{\alpha}})$; δ = gradient + field recovery delay; $0 \le \kappa \le T_a/t_{2,\max}$. Gradient strengths (durations): $G_s = 30$ G/cm (1.25 ms), $G_r = 29.6$ G/cm (0.125 ms). (a) Phase cycling for the *in-phase* MP-HNCA spectrum is $\phi_1 = y; \phi_2 = x, -x; \phi_3 = x; \phi_4 = 2(x), 2(-x); \phi_{rec.} = x, -x; \psi = y$. For the antiphase spectrum, ψ is incremented by 90°. (b) Phase cycling for the HN(CO)CANH experiment: $\phi_1 = x; \phi_2 = x, -x; \phi_3 = x; \phi_4 = 2(x), 2(-x); \phi_{rec.} = x, -x$.

In the proposed MP-HNCA experiment, the constant-time period in the $^{13}C^{\alpha}$ dimension is replaced by the real-time evolution. This has the following consequences. The $^{1}J_{C^{\alpha}C^{\beta}}$ coupling evolves during t_1, but as this period is usually kept short, sensitivity loss due to the $^{1}J_{C^{\alpha}C^{\beta}}$ modulation remains relatively small. Sensitivity losses due to $^{1}J_{C^{\alpha}C'}$ modulation are also minimized provided that $t_{1,\max} \le 7$ ms ($\sim 1/3J_{C^{\alpha}C'}$). Most importantly, the sensitivity costs due to rapid $^{13}C^{\alpha}$ transverse relaxation can also be minimized using the real-time evolution period. Thus, the coherence transfer efficiency for the MP-HNCA experiment can then be expressed as

$$\sin^2\!\left(2\pi^2 J_{NC^{\alpha}} T_a\right)\cos^2\!\left(2\pi^1 J_{NC^{\alpha}} T_a\right)\sin\!\left(2\pi^1 J_{NC'} T_b\right) \times \cos\!\left(\pi^1 J_{C^{\alpha}C'} t_1\right)\cos\!\left(\pi^1 J_{C^{\alpha}C^{\beta}} t_1\right)\exp\!\left(-2(T_a + T_b)/T_{2N}\right) \times \exp\!\left(-t_1/T_{2C^{\alpha}}\right). \quad [5]$$

Using the same transverse relaxation rates as given above, this yields coherence transfer efficiency of 0.043 for the *first*

t_1 *increment* in the *in-phase* experiment. For those residues, in which $^1J_{NC^\alpha}$ and $^2J_{NC^\alpha}$ are comparable, 10 and 9 Hz, the efficiency is 0.067 (Fig. 2c). It should be noted, however, that if spin-state selection is used to distinguish between inter- and intraresidual cross peaks, the overall sensitivity of cross peaks will be $\sqrt{2}$ times lower than in the in-phase experiment (*vide supra*). Coincidentally, the interresidual cross peaks that are of the same intensity as the intraresidual cross peaks also are more intense than other sequential connectivities. For this reason, it is advantageous to use the *in-phase* experiment for the general assignment of cross peaks and use spin-state-edited subspectra to distinguish between uncertain cross peaks (*12*). Thus, theoretically, the *in-phase* MP-HNCA experiment provides, as long as $t_{1,\max}$ is shorter than ~7 ms, virtually the same intensity as the conventional HNCA experiment, which we consider as the upper limit for coherence transfer efficiency.

The second alternative for obtaining sequential assignment in very large proteins is presented in Fig. 3b. This experiment is mostly similar to the HN(CO)CA experiment for its "out"-transfer part, and similar to the HNCA experiment for its "back"-transfer portion. The flow of coherence in this new hybrid experiment can be described as follows:

$$^1H^N - \{^1J_{H^NN}\} - {}^{15}N - \{^1J_{NC'}\} - {}^{13}C' - \{^1J_{C'C^\alpha}\} - {}^{13}C^\alpha(t_1) - \{^1J_{NC'}, {}^1J_{NC^\alpha}, {}^2J_{NC^\alpha}\} - {}^{15}N(t_2) - \{^1J_{H^NN}\} - {}^1H^N(t_3),$$

where t_i ($i = 1$–3) is an acquisition time for the corresponding spin and the couplings used for magnetization transfer are shown in parenthesis. In this particular experiment, the $^1H^N(i)$ magnetization is initially transferred to directly bond $^{15}N(i)$ spin. During the following delay $2T_N$, the magnetization is transferred to the interresidual $^{13}C'(i-1)$ spin. The desired magnetization is transferred further into the preceding $^{13}C^\alpha(i-1)$ spin. This can be described by the density operator $H_z^N(i)N_z(i)C'_z(i-1)C^\alpha_y(i-1)$ prior to the t_1 period. Subsequently, the $^{13}C^\alpha$ chemical shift is recorded during the t_1 evolution period as in the usual HN(CO)CA experiment, i.e., the magnetization can be described by the density operator $H_z^N(i)N_z(i)C'_z(i-1)C^\alpha_y(i-1)\cos(\omega_{C^\alpha(i-1)}t_1)\cos(\pi J_{C^\alpha C^\beta}t_1)$. The back-transfer step is similar to the familiar HNCA experiment, except that $^1J_{NC'}$ is refocused simultaneously with the $^2J_{NC^\alpha}$ coupling during the ensuing delay $2T_a$. Thus, after the ^{15}N chemical shift labelling period, which is employed as a semi-constant time TROSY manner (*20*), the desired magnetization can be described as $H_z^N(i)N_y(i)\cos(\omega_{C^\alpha(i-1)}t_1)\cos(\pi J_{C^\alpha C^\beta}t_1)$. Eventually the desired magnetization is transferred back to the amide proton using the sensitivity enhanced, gradient selected TROSY scheme presented by Yang and Kay (*19*). This results in only sequential cross peak that is modulated by the chemical shift of $^{13}C^\alpha(i-1)$ spin and $^1J_{C^\alpha C^\beta}$ coupling during the t_1 period. Again, if the evolution time is kept relatively short, no significant sensitivity loss occurs due to the $^1J_{C^\alpha C^\beta}$ modulation. The coherence transfer efficiency can be calculated by following the recipes described above:

$$\sin(2\pi {}^1J_{NC'}T_N)\sin(2\pi {}^1J_{NC'}T_a)\sin(2\pi {}^1J_{C'C^\alpha}T_C)\sin(2\pi {}^2J_{NC^\alpha}T_a) \times \cos(2\pi {}^1J_{NC^\alpha}T_a)\cos(\pi {}^1J_{C^\alpha C^\beta}t_1)\exp(-2(T_N+T_a)/T_{2N}) \times \exp(-2T_C/T_{2C'})\exp(-t_1/T_{2C^\alpha}). \quad [6]$$

The nominal values are: $^1J_{NC'} = 15$ Hz, $^1J_{NC^\alpha} = 10$ Hz, $^2J_{NC^\alpha} = 7$ Hz, $^1J_{C'C^\alpha} = 53$ Hz, $^1J_{C^\alpha C^\beta} = 35$ Hz, $2T_N \sim 33$ ms, $2T_a \sim 25$ ms, $2T_C \sim 9.1$ ms. The assumed transverse relaxation times for the ^{15}N, $^{13}C'$, and $^{13}C^\alpha$ spins are the same as above. By optimizing delay values, this gives coherence transfer efficiency of 0.037 for the *first increment*. The corresponding throughput is 0.046 if $^1J_{NC^\alpha} = 10$ Hz and $^2J_{NC^\alpha} = 9$ Hz (Fig. 2c). It is immediately apparent that the trick is to use rather efficient pathway from ^{15}N to $^{13}C'$ for the coherence transfer, and somewhat paradoxically, highly inefficient transfer from $^{13}C'$ to $^{13}C^\alpha$, in the first part of the sequence. On the contrary, during the latter part of the sequence, a more inefficient transfer from $^{13}C^\alpha$ to ^{15}N with respect to transfer from $^{13}C'$ to ^{15}N has to be used. It is then obvious that passive one-bond coupling between ^{15}N and $^{13}C^\alpha$ compromises the coherence transfer, i.e., $\cos(2\pi {}^1J_{NC^\alpha}T_a)$ dependence. The tradeoff is then made between two times longer $^{13}C'$–$^{13}C^\alpha$ INEPT transfer in the HN(CO)CA-type transfer, $\sin^2(2\pi {}^1J_{C'C^\alpha}T_C)\exp(-4T_C/T_{2C'})$, and compromised coherence transfer between ^{15}N and interresidual $^{13}C^\alpha$ spin in the HNCA-type transfer, $\sin^2(2\pi {}^2J_{NC^\alpha}T_a)\cos^2(2\pi {}^1J_{NC^\alpha}T_a)$, in both out- and back-transfer steps. If the TROSY works sufficiently well, i.e., the ^{15}N relaxation time is rather long ($T_{2,{}^{15}N} > 50$ ms), then the HN(CO)CA-type pathway will benefit from straightforward ^{15}N to $^{13}C'$ transfer. If the ^{15}N transverse relaxation is relatively fast, then it is necessary to shorten $2T_N$ delay in order to compensate for sensitivity losses due to relaxation. In that case the $2T_N$ and $2T_a$ delays are approximately equally long, and consequently direct ^{15}N to $^{13}C'$ is somewhat compromised with respect to $2T_a$. In the proposed experiment, the coherence transfer pathway is of HN(CO)CANH-type; i.e., it combines the best (worst) of both approaches described above. Theoretically its throughput is somewhat more efficient than that in the conventional HN(CO)CA experiment under the relaxation conditions considered. When the HN(CO)CANH experiment is compared to the proposed MP-HNCA experiment, it has two advantages: (*i*) there is no $^1J_{C'C^\alpha}$ coupling evolution during the t_1 period, which enables longer acquisition in t_1 without compromising the sensitivity, and (*ii*) it contains only interresidual cross peaks, that is, spectral overlap is not increased.

The proposed experiments were tested on 60.8-kDa homodimer of protein Cel6A (*21*) from the thermophilic soil bacterium *Thermobifida fusca* (286 amino acid residues), uniformly ^{15}N, ^{13}C labeled with >90% ^2H enrichment, 92/8% H_2O/D_2O, pH 6.0, in a 270-μl Shigemi microcell at 4°C. All experiments were carried out on a Varian UNITY INOVA 800 NMR spectrometer equipped with a $^{15}N/^{13}C/^1H$

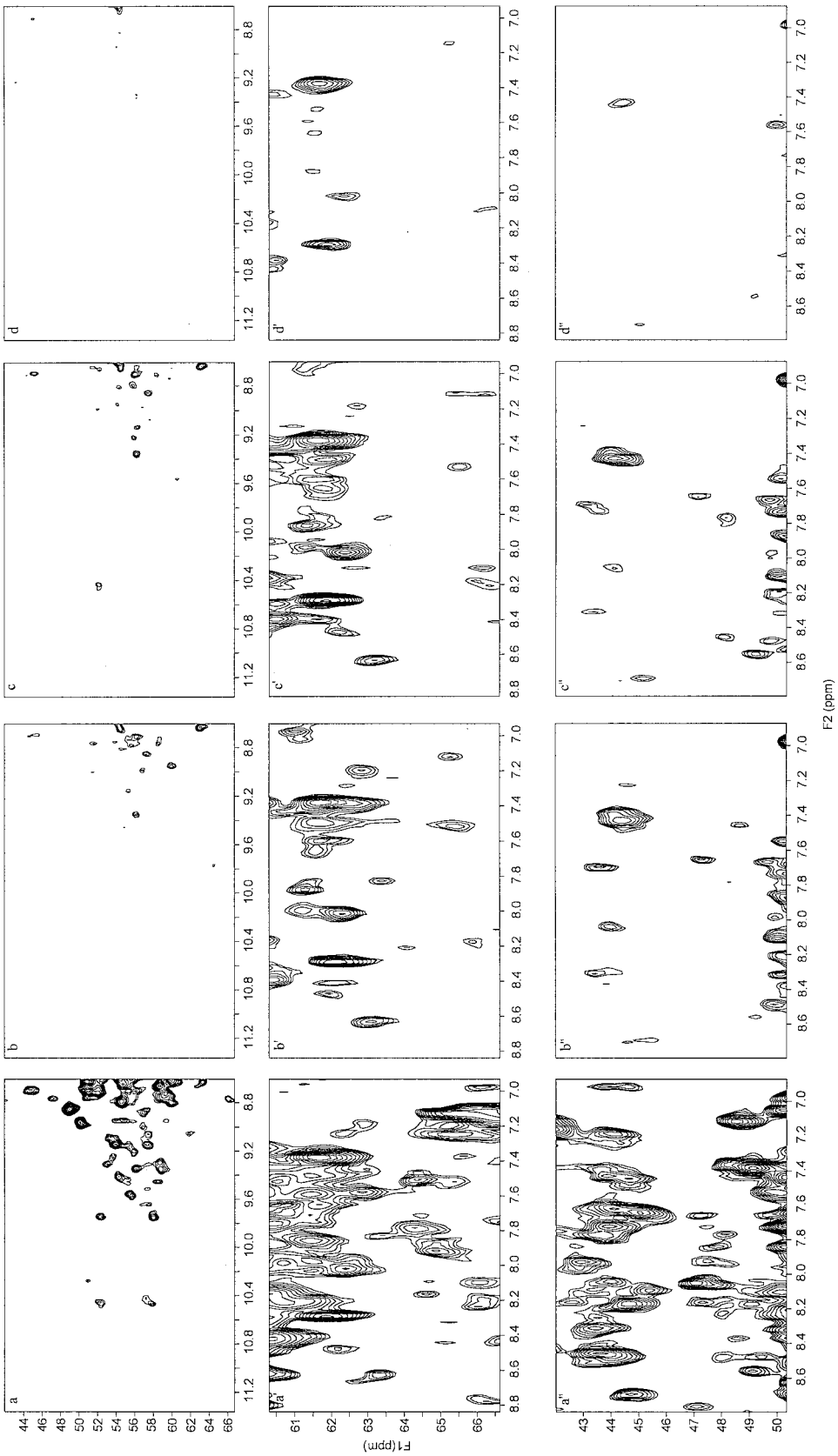

FIG. 4. Selected expansion from three different $^{13}C^{\alpha}$–$^{1}H^{N}$ regions of the in-phase MP-HNCA (*a*–*a*″), HN(CO)CA (*b*–*b*″), HN(CO)CANH (*c*–*c*″), and sequential HNCA (*d*–*d*″) spectra. All spectra were recorded using 128 transients per FID, with 34 and 512 complex points and the corresponding acquisition times of 6.9 and 43 ms in t_1 and t_3, respectively. A total acquisition time was 10 h per spectrum. The data were zero-filled to 2048 × 2048 points before Fourier transform and phase-shifted squared sine-bell window functions were applied in both dimensions.

triple-resonance probehead and an actively shielded triple-axis gradient system.

Figure 4 shows expansions from three selected regions from the first t_2 interferograms of the *in-phase* MP-HNCA(*a*–*a*″), HN(CO)CA (*b*–*b*″), and HN(CO)CANH (*c*–*c*″) and sequential HNCA (*d*–*d*″) experiments. In the *in-phase* MP-HNCA spectrum both intraresidual and sequential cross peak are visible, whereas only sequential cross peaks are visible in the sequential HNCA, HN(CO)CA, and HN(CO)CANH spectra. As can be seen, several interresidual cross peaks, which are absent in the HN(CO)CA spectrum, are visible in the proposed MP-HNCA or HN(CO)CANH spectra. However, some of the cross peaks are still more intense in the HN(CO)CA experiment. The sequential HNCA is not as sensitive as the other three experiments, because of the constant-time evolution period in t_1 (*vide supra*).

In conclusion, we have presented two new triple-resonance experiments facilitating sequential assignment of very large proteins. The proposed MP-HNCA experiment is the real-time variant of the original MP-CT-HNCA experiment, in which the constant-time $^{13}C^{\alpha}$ evolution period can seriously deteriorate available sensitivity due to the rapid $^{13}C^{\alpha}$ transverse relaxation and $^{1}J_{C^{\alpha}C^{\beta}}$ coupling during the constant-time period. Rapid $^{13}C^{\alpha}$ relaxation as well as compromised $^{1}J_{C^{\alpha}C'}$ refocusing hinders the also recently introduced sequential HNCA experiment with respect to the non-CT HN(CO)CA experiment. On the contrary, the proposed MP-HNCA experiment provides sequential connectivities without constant-time evolution period and is an attractive alternative to the assignment strategy based on the conventional HNCA/HN(CO)CA experiment pair. The second alternative, the HN(CO)CANH experiment, can be employed for obtaining sequential cross peaks using the novel "out and other way back" -type coherence transfer. It makes possible detection of merely sequential connectivitities without a costly constant-time t_1 evolution period or $^{1}J_{C^{\alpha}C'}$ evolution during t_1, by utilizing $^{1}J_{NC'}$ and $^{1}J_{C'C^{\alpha}}$ couplings for the "out"-transfer and $^{1}J_{NC'}$ and $^{2}J_{NC^{\alpha}}$ couplings for the "back"-transfer. Thus, it can be used for the assignment together with the conventional HNCA as a replacement for the HN(CO)CA. Theoretically this approach yields slightly more efficient coherence transfer than the conventional HN(CO)CA experiment and clearly outperforms the sequential HNCA or MP-CT-HNCA experiments in very large proteins. The presented experiments take full advantage of the TROSY techinique that works most efficiently at the highest field strengths available today (900 MHz), while they minimize sensitivity losses originating through $^{13}C'$–$^{13}C^{\alpha}$ INEPT transfers. The proposed experiments are optimal for the proteins and macromolecular complexes with rotational correlation time beyond 50 ns at the highest magnetic field strengths. These experiments can be expected to be useful for assignment of very large proteins produced utilizing segmental isotope labeling techniques (*22*) and for studying high molecular weight complexes beyond 60–70 kDa, in which the labeled protein itself is relatively small.

ACKNOWLEDGMENT

This work was financially supported by the Ministry of Education.

REFERENCES

1. G. Wider and K. Wüthrich, *Curr. Opin. Struct. Biol.* **9,** 594–601 (1999).
2. A. Bax and S. Grzesiek, *Acc. Chem. Res.* **26,** 131–138 (1993).
3. T. Yamazaki, W. Lee, M. Revington, D. L. Mattiello, F. W. Dahlquist, C. H. Arrowsmith, and L. E. Kay, *J. Am. Chem. Soc.* **116,** 6464–6465 (1994).
4. K. H. Gardner and L. E. Kay, *Annu. Rev. Biophys. Biomol. Struct.* **27,** 357–406 (1998).
5. K. Pervushin, R. Riek, G. Wider, and K. Wüthrich, *Proc. Natl. Acad. Sci. U.S.A.* **94,** 12366–12371 (1997).
6. M. Salzmann, K. Pervushin, G. Wider, H. Senn, and K. Wüthrich, *J. Am. Chem. Soc.* **122,** 7543–7548 (2000).
7. T. Yamazaki, H. Tochio, J. Furui, S. Aimoto, and Y. Kyogoku, *J. Am. Chem. Soc.* **120,** 872–880 (1997).
8. M. Sattler, J. Schleucher, and C. Griesinger, *Prog. Nuc. Magn. Reson. Spectr.* **34,** 93–158 (1999).
9. P. Permi and A. Annila, *Magn. Res. Chem.* **39,** 179–181 (2001).
10. S. C. Panchal, N. S. Bhavesh, and R. V. Hosur, *J. Biomol. NMR* **20,** 135–147 (2001).
11. D. Yang and L. E. Kay, *J. Am. Chem. Soc.* **121,** 2571–2575 (1999).
12. P. Permi and A. Annila, *J. Biomol. NMR* **20,** 127–133 (2001).
13. J. P. Loria, M. Rance, and A. G. Palmer III, *J. Magn. Reson.* **141,** 180–184 (1999).
14. A. Meissner, J. Ø. Duus, and O. W. Sørensen, *J. Biomol. NMR* **10,** 89–94 (1997).
15. M. Ottiger, F. Delaglio, and A. Bax, *J. Magn. Reson.* **131,** 373–378 (1998).
16. P. Andersson, J. Weigelt, and G. Otting, *J. Biomol. NMR* **12,** 435–441 (1998).
17. P. Permi, S. Heikkinen, I. Kilpeläinen, and A. Annila, *J. Magn. Reson.* **140,** 32–40 (1999).
18. A. Meissner and O. W. Sørensen, *J. Magn. Reson.* **150,** 100–104 (2001).
19. D. Yang and L. E. Kay, *J. Biomol. NMR* **13,** 3–9 (1999).
20. P. Permi, P. R. Rosevear, and A. Annila, *J. Biomol. NMR* **17,** 43–54 (2000).
21. M. Spezio, D. B. Wilson, and P. A. Karplus, *Biochemistry* **32,** 9906–9916 (1993).
22. T. Otomo, K. Teruya, K. Uegaki, T. Yamazaki, and Y. Kyogoku, *J. Biomol. NMR* **14,** 105–114 (1999).
23. A. J. Shaka, J. Keeler, T. Frenkiel, and R. Freeman, *J. Magn. Reson.* **52,** 335–338 (1983).
24. M. Piotto, V. Sauder, and V. J. Sklenar, *J. Biomol. NMR* **2,** 661–665 (1992).
25. S. Grzesiek and A. Bax, *J. Am. Chem. Soc.* **115,** 12593–12594 (1993).
26. D. Marion, M. Ikura, R. Tschudin, and A. Bax, *J. Magn. Reson.* **85,** 393–399 (1989).
27. P. Permi, T. Sorsa, I. Kilpeläinen, and A. Annila, *J. Magn. Reson.* **141,** 44–51 (1999).
28. D. Yang, R. A. Venters, G. A. Mueller, W. Y. Choy, and L. E. Kay, *J. Biomol. NMR* **14,** 333–343 (1999).